Linearized secondary-electron cascades from the surfaces of metals. I. Clean surfaces of homogeneous specimens

E. N. Sickafus
Research Staff, Ford Motor Company, Dearborn, Michigan 48121
(Received 18 October 1976; revised manuscript received 11 March 1977)

The cascade in the secondary-electron emission from atomically clean and atomically characterized surfaces of metals has been studied in the energy region of shortest inelastic mean free paths (10 eV $\lesssim E \lesssim$ 1000 eV). Specimen surfaces were cleaned *in situ* and characterized under ultra-high-vacuum conditions ($\sim 10^{-9}$ Torr) by low-energy electron diffraction and Auger electron spectroscopy. The cascade from clean surfaces was found to consist of linear segments when $\log j(E)$ was displayed vs $\log E$, where $j(E)$ is the emission current distribution as a function of the electron kinetic energy E. From the linear characteristic and the dependence of emission on primary beam energy E_p it is inferred that the emission current in the cascade is of the form $j(E) = A\ E^{-m}\ E_p^{-n}$. It is shown that this functional form is compatible with a solution of the Boltzmann diffusion equation. Deviations from linearity are found in the form of a segmented (linear) display where segmentation is caused by internal sources such as Auger electron sources. The linear segments are joined near energies characteristic of bound electrons in the solid. These effects are used to form the basis of a new approach to surface characterization.

I. INTRODUCTION

Several electron spectroscopies currently in use for the investigation of the solid-vacuum interface make use of spectral features that appear superimposed on the secondary-electron cascade as a background. The work reported here is motivated by the need to understand the relation between the secondary-electron cascade and superimposed spectral features.

The cascade in secondary-electron emission from atomically clean and atomically characterized surfaces of metals has been studied in the energy range of shortest inelastic mean free paths l_i. Data from various systems indicate that the smallest values of l_i in metals occur in the energy range of ~50 to ~500 eV.[1-3] In this energy range, l_i may approach atomic dimensions. It is, of course, this restriction of the magnitude of l_i which yields surface selectivity and enables an electron spectroscopy to be used as a surface tool. Therefore, if the condition of a surface can have an effect on the secondary-emission cascade it should be most perceptible in this energy range. Attention here is directed to the 10–1000 eV energy range of secondary-electron emission from a surface bombarded by a primary beam of electrons having an energy $E_p \leq 3$ keV.

The sensitivity to surface conditions of the cascade characteristic in the energy region of shortest inelastic mean free paths is demonstrated by the two spectra of Fig. 1. An Al(111) specimen was prepared by mechanical polishing, chemical etching, and final cleaning in alcohol to provide a highly polished surface. After mounting in the vacuum chamber and baking of the system an Auger spectrum was recorded as shown. A strong carbon peak is evident at 275 eV, an oxygen peak at 500 eV, and a small aluminum peak at 50 eV. The specimen next was sputter cleaned with argon ions to remove the carbon and oxygen. The second spectrum shows the result. It clearly is evident that surface conditions can have a pronounced effect on the cascade characteristic.

Studies of the cascade in secondary-electron emission have a variegated history.[4-6] Much of the work, however, predates the ultrahigh vacuum technology in current use and the studies generally have not benefitted from the associated

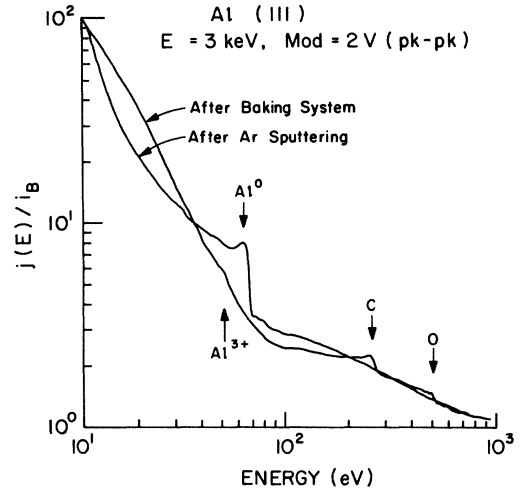

FIG. 1. Auger electron spectra of an Al(111) surface. The emission current $j(E)$ has been divided by the beam current i_B.

surface characterization tools. Consequently, surface conditions have been questioned. This has been noted, for example, in measurements of the cascade in cavity ionization associated with the slowing down of high-energy β particles[7] ($E_0 = 1.48$ MeV). The results were found to be in good agreement with theory except at low energies (spectra were examined for energies from a few eV up to 30 keV). Here, deviations from theory were attributed to unknown surface effects.

The nature of the secondary-electron cascade in metals, as evidenced in the region of the secondary-electron emission spectrum between the escape-probability-dominated emission at low energies and the rediffused primaries at high energies is discussed here. Emphasis is placed on the segmented linear characteristic that is obtained when the energy-dependent emission current[8] $j(E)$ is displayed in the $\log j(E)$ vs $\log(E)$ mode[9]; where E is the kinetic energy of an electron measured relative to the vacuum level. Deviations from linearity are evidence of various surface and bulk phenomena that are coupled to the secondary-electron cascade. In particular, such deviations distinguish surface- and subsurface-electron sources—the topic of the following paper referred to as II.

Extant reviews of secondary-electron emission[4,6,10,11] refer to the region of true secondaries as extending from the zero of energy (vacuum level) up to ~50 eV. As will be shown, the cascade can have a very broad range, more like $0 \leq E \lesssim \frac{1}{2}E_p$, when viewed in the $\log j(E)/\log(E)$ mode. In the conventional display mode, $j(E)$ vs E, it has been customary to divide the emission spectrum into three parts: (i) true secondaries, (ii) rediffused primaries, and (iii) the elastic peak. Here it is more convenient to divide the spectrum according to (i) the cascade, (ii) rediffused primaries, and (iii) the elastic peak. The separation between the cascade and the rediffused primaries is defined by a minimum in $j(E)$, labeled E_{cp}.

This is not the first time that the $\log j(E)$ vs $\log(E)$ display mode has been used. Although the data rarely are linear, this display mode is used commonly in presenting electron-slowing-down spectra associated with high-energy β sources.[5,7] Seah[12] seems to be the first to observe linearized cascade from a clean surface using the $\log j(E)$ vs $\log(E)$ display mode. He examined the secondary electron emission spectrum of polycrystalline silver in this mode, using a 300-eV primary beam incident at 70°, and demonstrated a linear behavior in the range $\sim 7 \leq E \lesssim 45$ eV—the range where true secondaries were expected. He obtained linearity in the lower ~5 eV of this range by adding an arbitrary constant to the retarding potential voltage so as to correct the retarding potential toward a value more representative of the electron energy inside the solid. Above 45 eV, his spectrum deviated rapidly from linearity. Sickafus[9] later showed that for a Ni(110) surface a similar result could be obtained with linearity extending to energies in excess of 1 keV. This appears to be the first evidence of a linearized cascade in the energy region of shortest inelastic mean free paths. He interpreted the deviation from linearity of the Ni spectrum near 50 eV to be a consequence of the low-energy tail of an Auger electron peak. In the Ni(110) spectrum several Auger electron peaks were found superimposed on a linear background. This observation became the basis of a technique for removing the true-secondary electron background from an Auger electron peak.[13]

The secondary-electron cascade has been the topic of several theoretical papers directed toward the secondary-emission line shape below 50 eV.[14-17] Certain assumptions were adopted for the lower energies which are somewhat restrictive at energies >50 eV. Nevertheless it will be seen that there is a reasonably good correlation between this restricted theory and the entire cascade as observed in the $\log j(E)/\log(E)$ mode.

Other theoretical treatments have addressed the higher-energy regions.[18,19] These theories have been applied to the excitation of internal electrons by the slowing down of high-energy β particles.[7] Here the electrons having a few tens of electron volts of energy are referred to as secondaries while the more energetic ones are called "δ rays." The theories deal with the δ rays. They derive from an integral equation representation of the statistical balance of electrons at all energy levels, the dynamics of which depend upon the scattering probabilities. Numerical solutions are obtained by using empirical scattering results.

Analytical solutions of the Boltzmann equation are of particular interest in describing the cascade because of the immediate insight they provide to the relationship between primary beam energy, inelastic scattering cross sections, multiple sources, escape probability, and general energy dependence. This was demonstrated first by Wolff[14] whose theory was later improved upon by Stolz.[15] Further analysis by Ritchie[20] has provided an analytical description of the coupled electron-hole cascade for energies very near the Fermi level.

Monte Carlo calculations also have been used to describe electron-slowing-down spectra. These have been compared with a numerical solution of the Boltzmann equation in the energy region of the electron-hole cascade and show good agreement.[21]

At much higher energies, they have been compared with experiment and the Spencer-Fano theory and show better agreement with the latter.[21]

The experimental technique is summarized in Sec. II. Following that a brief review of the theory of the secondary-electron cascade is given in Sec. III along with extensions of the theory which are of interest in these experiments. The experimental results are presented in Sec. IV. These results are interpreted in light of the existing theory and discussed in Sec. V.

II. EXPERIMENTAL TECHNIQUE

Three types of single crystal metallic specimens have been studied; Ni(110), Ni(111), Mg(111), Al(110), Al(111), and Al (polycrystalline). The samples all were cut from single-crystal bars using a commercial spark cutter. They then were polished mechanically by standard metallographic techniques, and finally, were polished chemically or electrochemically. The specimens were mounted in an ultrahigh-vacuum system on a goniometer where they were held in place by tantalum-metal clips which are extensions of a tantalum strip that served as a heater. The polycrystalline sample was obtained by melting and resolidifying, *in situ*, an Al single-crystal sample. The specimens were heated by passing a current through the tantalum-foil holder and their temperature was monitored via a thermocouple imbedded in a hole in the side of each specimen. *In situ* cleaning techniques were used which included heating, ion-sputter cleaning, and chemical reactions with high-purity oxygen or hydrogen.

Secondary-electron spectra were obtained as backscattered spectra from a polished metal surface in an ultrahigh-vacuum system. Two different commercial four-grid low-energy electron-diffraction systems were used.[22] Their low-energy-electron diffraction (LEED) optics provided spherical-sector grids which served as retarding potential analyzers.

The usual methods of potential modulation analysis, typical of Auger electron spectroscopy,[23,24] were employed. The modulation amplitudes were usually in the range of 6–8 V (peak to peak). The $\log j(E)/\log(E)$ plots were found to be linearly related to modulation amplitude in this range (and lower modulation) for all values of $\log(E)$. To obtain $\log j(E)$ vs $\log(E)$ displays the output of the lockin amplifier, $j(E)$, and a signal proportional to the retarding potential voltage (representing an arbitrary fraction α of E where $\alpha = 10^{-3}$), both were processed by analog type of logarithmic amplifiers (Burr Brown, 4008–60 dB) before being displayed on an xy recorder. Further details of electronic circuitry are given in II.

Electron bombardment of the specimens could be done with either the LEED electron gun which was coaxial with the analyzer (LEED optics) or with a "glancing incidence" electron gun that was oriented ~75° from the analyzer axis. The spectra shown here were taken with the glancing incidence electron gun, and with the specimen tilted ~20° away from the analyzer axis toward the glancing incidence gun, unless specified otherwise.

Pressure in the vacuum chamber was usually in the mid 10^{-9} Torr range while making secondary-electron-emission measurements. During sputter cleaning with argon gas, the chamber was valved off from the main pump. It was noted that this procedure permitted the partial pressure of CO to rise to values greater than that of the argon; e.g., $P(\mathrm{CO})/P(\mathrm{Ar}) \sim 5$. After sputtering under these conditions a carbon deposit was always found on the specimen surface. However, by operating in the main chamber an auxiliary titanium sublimation pump shielded by a cylindrical liquid-nitrogen-cooled shroud, the pressure of CO could be reduced greatly; e.g., $P(\mathrm{CO})/P(\mathrm{Ar}) \sim 10^{-7}$. In this case, sputter cleaning left no traces of surface carbon. Furthermore, an aluminum specimen could be sputter cleaned of all surface oxygen as determined by conventional Auger electron spectroscopy techniques. The surface of the *in situ* melted Al specimen then remained clean of oxygen, in an ambient pressure of $\sim 10^{-9}$ Torr for periods of up to five days provided that the CO partial pressure was negligible.

III. THEORETICAL CONSIDERATIONS

A. General nature of secondary-electron emission

Shown schematically in Fig. 2 is an idealized secondary-electron-emission spectrum in the $\log j(E)/\log(E)$ display mode. It is hypothesized that this is the characteristic spectrum to be associated with a monoenergetic ($E = E_p$) external source in the absence of all internal sources (e.g., Auger electron sources, characteristic losses, etc.) or sinks. The spectrum is divided into three sections: the secondary-electron cascade, rediffused primaries, and the elastic peak. As suggested in the figure, the rediffused primaries can be visualized as continuing with decreasing numbers to energies below E_{cp}, likewise, the cascade can be extended (linearly) up to E_p. Thus the boundary, E_{cp}, represents the region where one distribution begins to exceed the other. At the low-energy end of the secondary cascade a pronounced deviation from linearity occurs where the escape probability, $P(E')$ (E' is the energy of an internal electron relative to the bottom of the

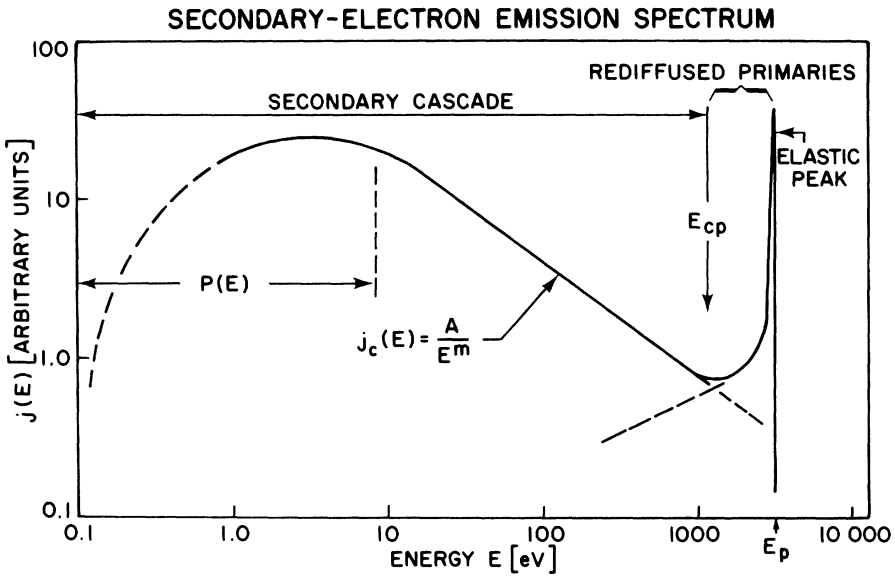

FIG. 2. Schematic representation of the backscattered secondary-electron spectrum associated with an (isolated) external source of monoenergetic electrons of energy E_p. This $\log j(E)$ vs $\log (E)$ display mode emphasizes the separation of the spectrum into three parts: (1) the secondary cascade bounded at high energies (at E_{cp}) by (2) rediffused primaries which are bounded by (3) the elastic peak. At low energies the cascade is attenuated by the escape probability $P(E)$.

band), becomes a strong effect, reducing the emission to zero at the zero of energy.

B. Cascade theory

Upon entering a metal an energetic electron is subjected to a sequence of inelastic and elastic scattering events. These events erode the primary electrons energy and alter its momentum until it either exits the solid at a surface or becomes trapped in the valence band. The significant inelastic events are two-electron processes in which the primary electron loses a discrete amount of energy to an electron of the solid giving rise to two electrons in excited states. Both of these electrons are then subject to similar scattering events. Thus is born the cascade process which is characterized by population probabilities that increase in magnitude with decreasing energy. The process continues until all excess electrons have escaped the solid and the remaining electrons have settled back into the Fermi sea.

The electron scattering process can be described in terms of two characteristic lengths; an elastic mean free path, $l_e(E')$, and an inelastic mean-free path, $l_i(E')$. The externally observed energy-dependent emission current $j(E)$ can be visualized as a depth-dependent sampling of an internal distribution function $N(x,E')$ where $0 \le x \le l_i(E')$. That is, it can be visualized as a sampling of the internal distribution function lying within an inelastic mean free path of the surface (see Paper II). Thus, the depth of sampling is energy dependent according as $l_i(E')$ is energy dependent. The externally observed sample of the internal-distribution function also is modified by boundary conditions imposed on the escaping electrons. The external current leaving a surface, $j(E,\alpha)$, is related to the internal current approaching the surface $j(E',\beta)$, by an escape probability $P(E')$ which, for an isotropic internal source, is given by[14]

$$P(E',\beta) = 1 - (W/E' \cos^2\beta)^{1/2}, \quad W \le E' \le E_p, \quad (1)$$

where W is the inner potential, and α and β are, respectively, the internal and external angles measured between the velocity vector and the corresponding normal to the surface.

Wolff[14] applied the Boltzmann diffusion equation to the description of the secondary-electron cascade. He cautions that the assumptions made limit its applicability to energies less than 100 eV. Nevertheless, this theory is reviewed here because first of all it has a clearly defined foundation which encompasses all of the basic physical processes that appear needed for a complete description of the problem. It serves our needs in that, although it is an approximate solution, it describes the cascade in an analytical form. This conveniently makes transparent the relationship between the emission current at the surface, the primary beam current, multiple sources, and the energy dependence of the cross section model employed. Secondly, although restrictive assumptions were invoked to facilitate solution of the differential-integral equation, Wolff's solution seems to have properties that carry over to higher energies than originally anticipated. It is possible, of course, that some of the apparent agreement between Wolff's theory and the experimental results described herein is fortuitous. Further theoretical analysis may be needed to settle that point.

In this treatment of the cascade theory $N(\vec{r},\vec{\Omega}'$,

$E', t)$ is the number of internal electrons, located within $d\vec{r}$ at $\vec{r}$ having velocities $\vec{v}$ within the direction $d\vec{\Omega}'$ at $\vec{\Omega}'$, and energy within dE' of E', at time t. This distribution function is required to satisfy the Boltzmann diffusion equation:

$$\frac{\partial N}{\partial t} + \vec{v} \cdot \nabla N = -\frac{vN}{l_i} + S + \int dE'' \int \frac{d\Omega'' v'' N F}{l_i}, \quad (2)$$

where $S = S(\vec{r}, \vec{\Omega}', E', t)$ is a source function, $l_i = l_i(E)$ the inelastic mean free path, and $F = F(\vec{\Omega}', E'; \vec{\Omega}'', E'')$ is the probability that an electron initially at $\vec{\Omega}'', E''$ will be found after scattering at $\vec{\Omega}', E'$. By treating the steady state and assuming a negligible gradient of N near the surface, this equation can be simplified to

$$\psi_l(E') = \int_{E'}^{\infty} dE'' \, F_l(E', E'') \psi_l(E'') + S_l(E'), \quad (3)$$

where $\psi_l(E') = vN_l/l(E')$, and the subscripts l designate Legendre polynomials of N, S, F, and ψ. This description assumes further a planar surface with a normally incident primary beam and enforces cylindrical symmetry.

To solve Eq. (3) Wolff made several assumptions: He assumed that a screened Coulomb potential was adequate to describe electron-electron scattering. He found that at low energies s-wave scattering predominates. He therefore assumed that electron-electron scattering is spherically symmetric (in the center of mass system) up to ~100 eV. Hence, on an average, an electron ($E' < 100$ eV) loses about half of its energy with each collision. The motion of the conduction electrons, compared with those in the cascade, was ignored. He concludes that at sufficiently low energies scattering produces a spherically symmetric distribution and consequently concentrates on ψ_0 and ignores higher harmonics. With these assumptions and an approximate allowance for the effect of exclusion on F_0, the secondary-emission current is given by the following expression:

$$j(E) = \frac{P(E)}{\eta_c \sigma_0(E)(1 - \frac{7}{5} E_F/E)} \left(\frac{E_p}{E}\right)^X. \quad (4)$$

In this equation, $\sigma_0(E)$ is the inelastic electron-electron scattering cross section, E_F is the Fermi energy, and η_c the number density of conduction-band electrons. The factor containing E_F is designed to alter σ_0 to an effective cross section as a result of the exclusion principle. The exponent X is energy dependent below $E \sim 4E_F$ and essentially is constant for greater energies: $X \cong 2$, $E \gtrsim 4E_F$.

This theory, Eq. (4), was compared by Wolff with experimental results of secondary-electron emission from Li with $E_p = 80$ eV and from Ag with $E_p = 155$ eV. These comparisons extended up to $E = 60$ eV. Since the publication of this theory, other improved calculations have been published,[15-17] but in none of these has there been an attempt to extend significantly the energy range of the cascade theory. It is of interest, therefore, to examine the implications of Eq. (4) when it is extended to high energies.

Consider $E \gg E_F$: At such energies the factor $P(E)$ in Eq. (4) and the factor containing E_F make negligible contributions to $j(E)$. Hence, at larger energies $j(E)$ is proportional to $[\sigma_0(E)E^x]^{-1}$. We can assume that the general behavior of $\sigma_0(E)$ is of the Bethe form,[25] $E^{-1}\log E$, and thus write

$$j(E) = CE_p^x / E^{x-1} \log E, \quad (5)$$

where C is a constant, or

$$\log j(E) = x \log E_p - (x-1)\log E - \log\log E + \log C. \quad (6)$$

Since $\log\log E$ is a slowly varying function on a given range of E, Eq. (6) is a linear function of slope $-(x-1)$.

We conclude that according to this theory, Eq. (6), an external source ($E_p \gg E_F$) generates secondary emission ($E > E_F$) whose cascade has a linear characteristic in the $\log j(E)/\log(E)$ mode. The slope of the characteristic curve is negative and has a magnitude ~1. Also a $\log j(E)$ vs $\log E_p$ display at constant E will have a linear characteristic.

C. Cascade dependence on E_p

A basic property of the cascade is that its linearity in $\log j(E)$ vs $\log(E)$ is independent of the primary beam energy E_p. As is evident from Eq. (6) the general effect of E_p is to raise or lower the linear cascade as E_p is increased or decreased, respectively. The range of the cascade (not contained explicitly in the theory) does, however, depend on E_p. That is, the boundary E_{cp}, shown in Fig. 2, shifts with the magnitude of E_p.

An important observation is the dependence of $j(E)$, at a given E, on E_p. Again, from Eq. (6), it is evident that a linear characteristic is to be expected from a display of $\log j(E)$ vs $\log E_p$ at a given E. This effect is found experimentally as shown in Sec. IV. This observation forms the basis for a "step correction" to Auger line shapes—a procedure that we presently are investigating.

D. Angular dependence of the cascade

Early studies of secondary-electron emission demonstrated that the angular emission at very low energies (~10 eV) is nearly cosinelike.[26] This result is of particular interest because a cosine emission is indicative of an isotropic internal dis-

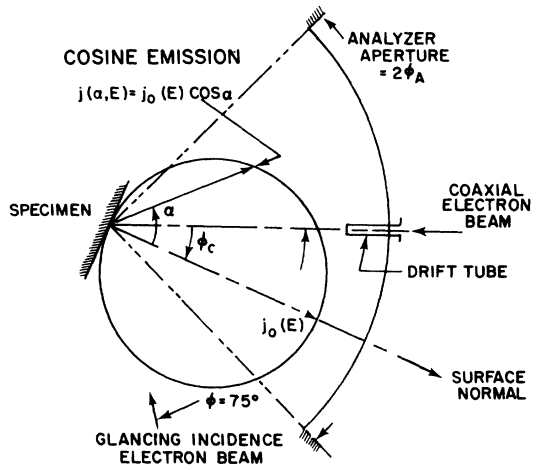

FIG. 3. Schematic illustration of the spatial relationship between a cosinelike emission plume, from a specimen whose surface normal is tilted through an angle ϕ_0, and the entrance aperture of a retarding-potential analyzer.

tribution function. On the other hand, recent studies have found certain Auger electron emission to have a complex angular dependence.[27] Since the cosinelike emission was observed at such low energies, near the peak of the secondary-electron cascade (see Fig. 2), it can be expected that cascade electrons dominated the detected current and Auger sources had little net effect. It may result, therefore, that cascade electrons can be characterized further as having an isotropic distribution. This was, of course, an assumption of the Wolff theory.

The experiments discussed here involve retarding potential analyzers having rather large apertures. Consequently, they are not useful for detailed angular studies. On the other hand, since the apertures do not intercept all of the secondary emission, there will be net angular effects that may correlate with particular angular emission functions. The case of a cosinelike emission will be examined in particular.

The observed spectral signal is a partial integral of the angular emission,

$$j(E)=\int_{\Omega_A} j(\alpha,E)\,d\alpha, \tag{7}$$

where Ω_A is the solid angle of the analyzer aperture ($\Omega_A \sim \pi/2$ sr) and α is the angle of emission (see Fig. 3). By tilting the specimen through an angle ϕ_0 a different integral of $j(\alpha,E)$ is found. Thus, if the emission follows a cosine law, i.e., $j(\alpha,E)=j_0(E)\cos\alpha$, then tilting the specimen couples differing amounts of the cosine plume to the analyzer aperture as illustrated in Fig. 3. The corresponding analyzer current is given by

$$j(E,\phi_0)=j_0(E)\int_0^{\pi}(\cos^2\Theta_m-1)\,d\gamma, \tag{8}$$

where Θ_m is a function of γ and ϕ_0 such that

$$\cos\Theta_m(\gamma,\phi_0)=-\frac{\cos\Theta_A\cos\phi_0+\sin\phi_0\cos\gamma(\sin^2\phi_A+\sin^2\phi_0\sin^2\gamma)^{1/2}}{1-\sin^2\phi_0\sin^2\gamma} \tag{9}$$

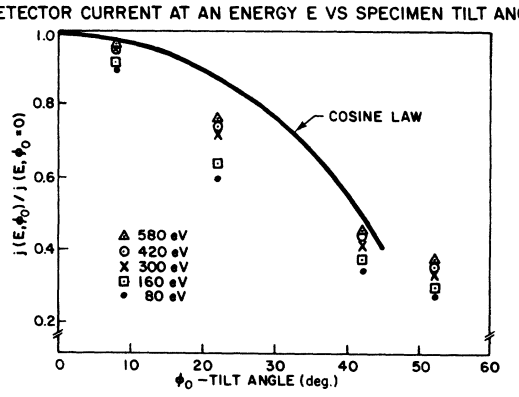

FIG. 4. Plot of $j(E,\phi_0)/j(E,\phi_0=0)$ vs the tilt angle ϕ_0 of the specimen relative to the analyzer axis. The curve is a calculated result corresponding to cosine emission. The vertical series of data represent values measured at different energies (see code in the figure) on the spectra shown in Fig. 7.

for $\phi_0 \leq \phi_A$. Θ_m is the maximum polar angle of an element of emission current at a given angle γ, that is, where the polar angle relative to the surface normal intersects the aperture, and γ is the azimuthal angle of the current element measured relative to the plane containing the surface normal and the analyzer axis (the plane of Fig. 3). Equation (9) does not take into account the shadow of the drift tube that shields the coaxial electron gun—a lesser correction. Equation (9) has been evaluated numerically and the results scaled to $j(E,\phi_0=0)$. These results are shown as the continuous curve in Fig. 4.

E. Sources and sinks

The effect of multiple sources ($+S$) and sinks ($-S$) can be derived from Wolff's results. The source term of the Boltzmann equation, $S(\vec{r},\vec{\Omega}',E',t)$ in Eq. (2), represents the density of internal

secondaries produced by the primaries passing locations $\vec{r}$. In the integral equation for ψ_l, as given by Eq. (3), S_l has been limited to an energy-dependent function, and it is an additive term in the equation for ψ_l. Following Wolff's approach in which the motion of the conduction electrons is ignored, relative to that of the cascade electrons, the function F_l in Eq. (3) can be expressed as

$$F_l(E', E'') = (2/E'')P_l(E'/E'')^{1/2} \tag{10}$$

and then Eq. (3) becomes

$$\psi_l(E') = 2\int \frac{dE''}{E''} P_l\left(\frac{E'}{E''}\right)^{1/2} \psi_l(E'') + S_l(E'). \tag{11}$$

The homogeneous equations yield solutions

$$\psi_l \sim E'^{\alpha_l}, \tag{12}$$

where $\alpha_0 = -2$, $\alpha_1 = -\frac{3}{2}$, etc. When $S_l(E')$ is known the complete solution of Eq. (11) is given by

$$\psi_l(E') = -\int_{E'}^{\infty} \left(\frac{E'}{E''}\right)^{\alpha_l} \frac{\partial S_l}{\partial E''} dE''. \tag{13}$$

We can now apply Eq. (13) to the problem of multiple sources and sinks. Consider a homogeneous source of strength S_p associated with the primary beam and an auxiliary source (sink) of strength $\pm S_A$ associated with an internal excitation at an energy E_A, where $E_A < E_p$. Then the source term of Eq. (11) can be written as

$$\begin{aligned} &S_0(E') = S_p\delta(E' - E_p') \pm S_A\delta(E' - E_A'), \\ &S_l(E') = 0, \quad l \neq 0, \end{aligned} \tag{14}$$

where $\delta(E' - E_j')$ is the Dirac δ function. On substitution of Eq. (14) into Eq. (13) and then using Wolff's expression for $l(E')$,

$$l(E') = 1/\eta_c\sigma_0(E')(1 - \tfrac{7}{5}E_F/E') \tag{15}$$

and for $P(E)$, Eq. (1), we obtain for $j(E) = Nv = \psi_0(E')l(E')$ the following:

$$j(E) = \frac{-\alpha_0 E^{\alpha_0} P(E)}{\eta_c\sigma_0(E)(1 - \frac{7}{5}E_F/E)} \left(\frac{S_p}{E_p^{\alpha_0+1}} \pm \frac{S_A}{E_A^{\alpha_0+1}}\right), \tag{16}$$

for $E < E_A$ and

$$j(E) = \frac{-\alpha_0 E^{\alpha_0} P(E)}{\eta_c\sigma_0(E)(1 - \frac{7}{5}E_F/E)} \left(\frac{S_p}{E_p^{\alpha_0+1}}\right), \tag{17}$$

for $E_A \leq E < E_p$. Applying again the arguments used in conjunction with Eq. (15) and substituting $\alpha_0 = -2$ we obtain from Eq. (16)

$$j(E) = (2/\eta_c E \log E)(E_pS_p \pm E_AS_A) \tag{18}$$

for $E < E_A$ and a similar equation for $E_A \leq E \leq E_p$, but without the term $\pm E_AS_A$. Thus the effect of an auxiliary source (sink) is to "turn on" or "turn off" the term $\pm E_AS_A$ in Eq. (18) depending on whether $E > E_A$ or $E < E_A$. This term does not affect the energy dependence of $j(E)$, but does alter its strength in a multiplicative fashion. In the logarithmic form Eq. (18) becomes

$$\begin{aligned} \log j(E) = {} &\log(2/\eta_c) - \log\log E \\ &+ \log(E_pS_p \pm E_AS_A) - \log E. \end{aligned} \tag{19}$$

for $E < E_A$ or with $S_A = 0$ if $E_A < E < E_p$. Thus a source (sink) is recognized as a positive step (negative for a sink) in $\log j(E)/\log(E)$ on passing from $E > E_A$ to $E < E_A$. Since $\log(E_pS_p \pm E_AS_A)$ is a constant it simply causes a parallel shift of the cascade in the $\log j(E)/\log(E)$ mode on crossing $E = E_A$. The magnitude of the shift is a measure of the strength of the source or sink. It is evident then that a step in a linearized cascade can derive from adding the cascade produced by an internal source to the cascade produced by an external source, or by adding independent internal cascades.

The above analysis has followed closely the work of Wolff in the zeroth-order Legendre polynomial. Emphasis on the lowest-order polynomial is related to the conclusion that at low energies the internal electron distribution is spherically symmetric. In the analysis, the lower the energy the more ψ_0 overwhelms the higher-order polynomials. Thus, in comparing these theoretical results with experimental observations we in effect are emphasizing correlations related to isotropic internal distributions. Furthermore, by ignoring the gradient of the distribution function in the Boltzmann equation one assumes a homogeneous distribution. Along with this we have assumed tacitly a homogeneous source function. These obvious limitations do not nullify the analysis as applied here. Although more critical analyses may be pursued in the form of integral differential equations, the transparancy of Wolff's closed-form solution is readily appreciated.

IV. EXPERIMENTAL RESULTS

As indicated in Fig. 2 the linear behavior of the secondary-electron cascade in the $\log j(E)/\log(E)$ mode results in $j(E)$ varying as an inverse power of E, see Eq. (5), where E is the kinetic energy of the electrons. In this paper, E is equated to the retarding potential of the analyzer, and consequently, within a contact potential correction, E is the energy relative to the vacuum zero rather than the energy relative to the bottom of the band.

The linear nature of the cascade is evident in Fig. 5, where a Ni(110) secondary-electron spectrum is shown in the $\log j(E)/\log(E)$ mode.[28] This spectrum was produced by a 3 keV primary beam near glancing incidence. The thresholds of possible core-state ionizations leading to Auger-elec-

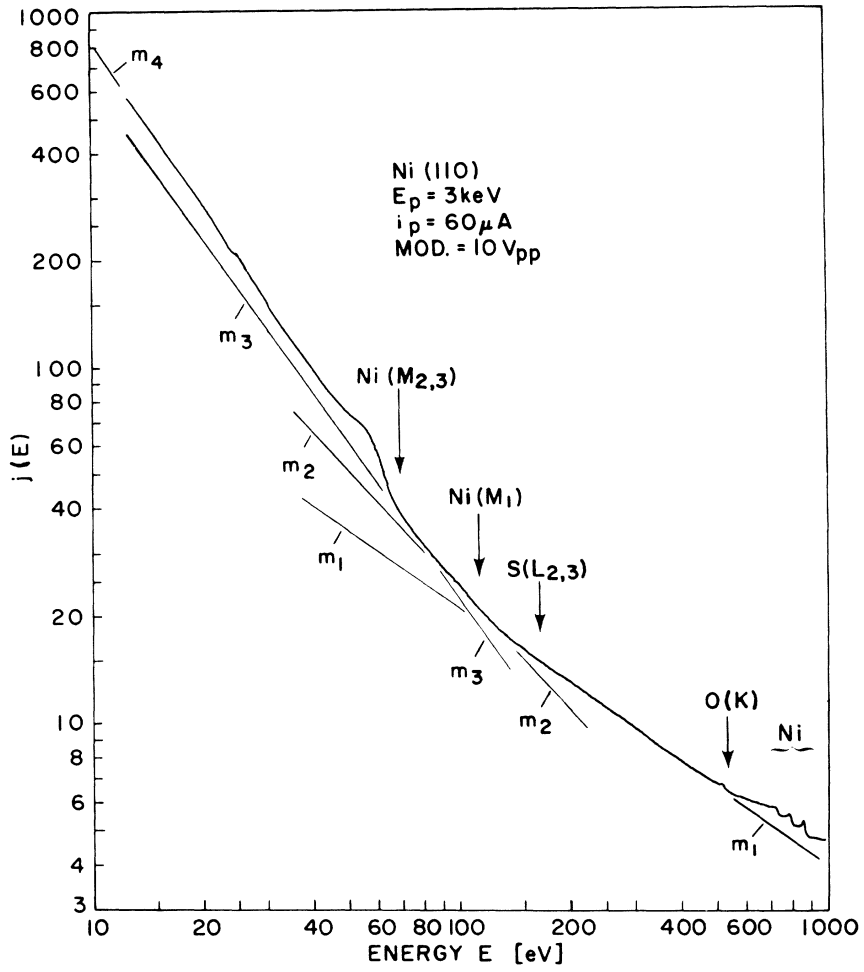

FIG. 5. Log $j(E)$/log (E) display of the cascade region of emission from a Ni(110) surface bombarded by an off-axis, 3 keV beam of electrons. Several linear segments are indicated by extensions of their slopes labeled $m_i (i = 1, 2, 3, 4)$. The binding energies of various electron levels are indicated. The dip in the curve at 24 eV is an instrumental effect associated with changing ranges of the lockin amplifier during curve tracing.

tron emission are indicated in the figure. Auger peaks clearly are evident in the figure: Ni (855, 790, 710, eV) and O (510 eV). Linear regions also are evident and these are labeled, m_1, m_2, m_3, and m_4, where m_1 characterizes the cascade following the oxygen Auger peak, m_2 and m_3 characterize cascade-slope changes following the S($L_{2,3}$) and Ni(M_1) thresholds, respectively, and m_4 characterizes the cascade following the low-energy Ni Auger peak.

The steplike nature of the cascade caused by an internal source is evident in Fig. 5 following the low-energy Ni peak. A short range of the cascade ~42 to 48 eV, appears to be parallel to m_3 and then toward lower energies the slope m_4 dominates. Other examples of the linear nature of the cascade in the log$j(E)$/log(E) mode are evident in the remaining figures of this paper and in II.

The reason for extending the linear cascade to E_p in Fig. 2 is that the cascade function appears to be independent of E_p. This is illustrated in Fig. 6. Here are shown these three spectra for different primary beam energies $E_p = 1$, 2, and 3 keV. Note that as E_p is increased with constant primary beam current i_p the secondary cascade decreases in intensity but remains constant in slope. The decrease in intensity is consistent with a redistribution of a fixed number of electrons over a broader range of energy. Another way of looking at this effect is to assert that the cascade electrons are sufficiently thermalized with the lattice that they do not know the source responsible for them. It is found, as expected, that the intensity of the cascade at a given energy is proportional to the primary beam current.

As seen in Fig. 6 the boundary E_{cp} increases with increasing E_p. In the region of rediffused primaries the emission function $j_{rp}(E)$ changes so as to join smoothly with $j_c(E)$ near the minimum at E_{cp}. This function and effects in this region are not discussed here except to note that $j_{rp}(E)$ along with the elastic peak provide an indication of the strength of high-energy sources, in the range $E_{cp} \leq E \leq E_p$, that can produce secondary-cascade electrons.

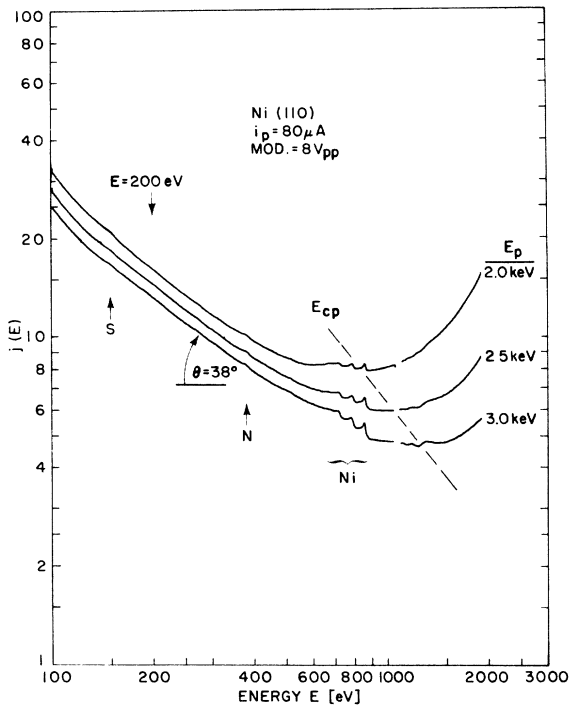

FIG. 6. Dependence of the cascade-rediffused primary boundary, E_{cp}, on primary beam energy is illustrated in these log $j(E)$/log (E) spectra from a Ni(110) surface. Internal sources due to Auger electron transitions are labeled for sulfur, nitrogen, and nickel.

The angular dependence of the cascade was examined by tilting the specimen through an angle ϕ_0 and displaying the corresponding log$j(E, \phi_0)$/log(E) curves. These spectra are examined in light of the discussion in Sec. III D. In Fig. 7, are shown spectra obtained with different orientations ϕ_0 of the specimen normal relative to the analyzer axis. These spectra were obtained with a 3-keV primary beam from the glancing incidence electron gun. Over the range of energies shown (40–1000 eV) the spectra are offset approximately parallel to one another with different tilt angles. That is, the major effect of tilt on the net current is to scale the current by a constant factor that is approximately independent of energy.

There are systematic angular effects among the spectra of Fig. 7. One of these is demonstrated in Fig. 4 where the ratios of currents at a given energy have been computed with respect to the $\phi_0 = 0$ curve at the five energies shown by the lower set of arrows in Fig. 4. Note that at each angle there is a vertical spread of ratio values with the lowest point corresponding with the smaller energy and the uppermost point corresponding with the larger energy. The intermediate points in a vertical group are distributed according to their respective energies. For comparison, the values to be expected for cosine-law emission, as given by Eqs. (8) and (9), are indicated by the curve plotted in Fig. 4. It is evident from Fig. 3 that there is somewhat less tilt-angle effect on the higher-energy electrons than on those at the lower energies. Also noted is the tendency of the higher-energy electrons to follow more closely the cosine-law curve.

Another systematic angular dependence of the data in Fig. 7 is related to Auger electron emission. The Auger peaks for N (380 eV), O (510 eV), and Ni (710, 780, and 850 eV) are more sharply defined in the $\phi_0 = 0$ spectrum than in the others. The definition decreases with increasing angle and is worst for $\phi_0 = 52°$. For example, the peak to background ratio for the Ni (850 eV) peak decreases as, 1.16 ($\phi_0 = 8°$), 1.13 ($\phi_0 = 22°$), 1.11 ($\phi_0 = 42°$), and 1.10 ($\phi_0 = 52°$). This is a well-known phenomenon that is attributed to the generation of greater numbers of Auger electrons near the surface with increasing angle of incidence (decreasing ϕ_0) of the primary beam.

As mentioned above, tilting the specimen causes the log$j(E)$/log(E) curves to be shifted approximately parallel to one another. Hence, the major effect is to alter the magnitude of $j(E)$ and not its

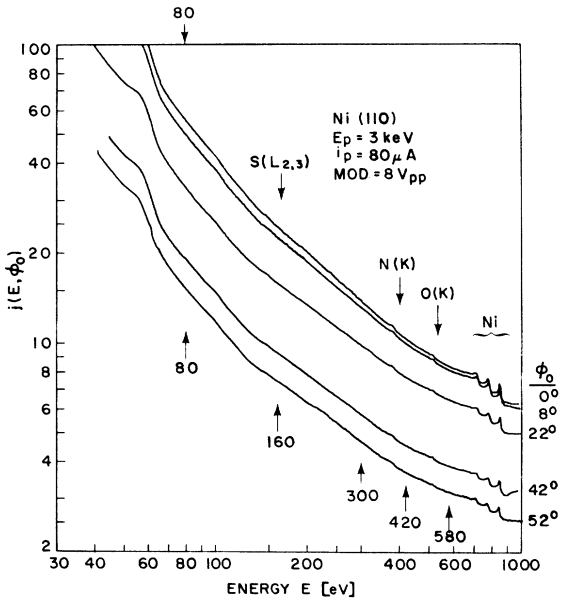

FIG. 7. Dependence of log $j(E)$/log (E) displays on the angle of tilt ϕ_0 of the specimen relative to the retarding potential analyzer axis for emission from a Ni(110) surface. The angles of tilt are indicated in the right-hand margin next to each curve. Auger peaks for nitrogen, oxygen, and nickel are labeled along with the binding energy of sulfur $L_{2,3}$ electrons. The slopes of these curves, measured at the energies labeled with upward pointing arrows, are plotted in Fig. 8.

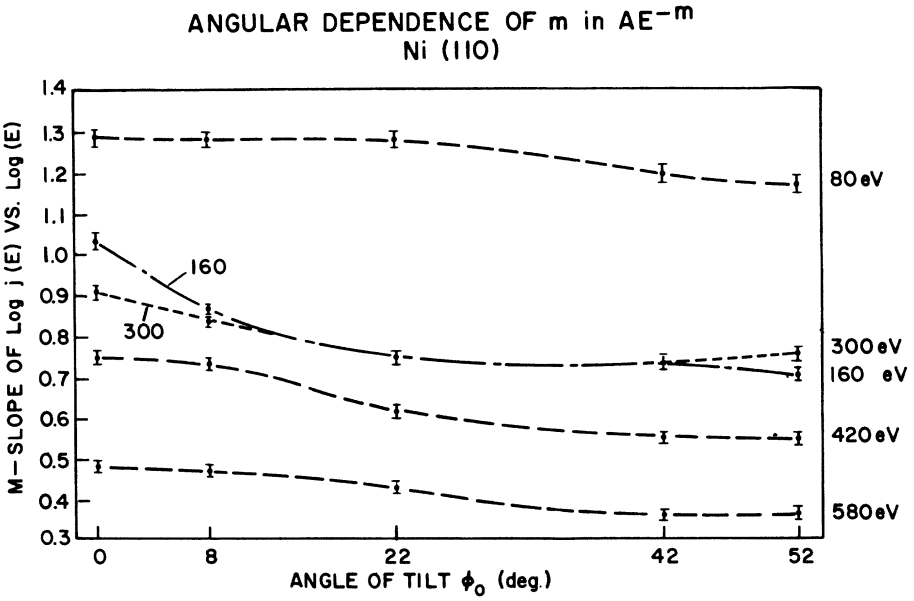

FIG. 8. Relationship of the slopes of the log$j(E)$/log (E) curves of Fig. 7 at the energies labeled in Fig. 7 are shown here as a function of the angle of tilt ϕ_0 of the specimen relative to the retarding-potential analyzer axis. Error bars indicate the uncertainty of measuring the slopes.

functional form. There is, of course, some alteration. This is illustrated in Fig. 8 where the slopes m of the log$j(E)$/log(E) curves in Fig. 6 are plotted for the several energies indicated. The error bars indicate the uncertainty in judging the tangents of the curves. Some dependence of m on ϕ_0 is apparent, but it is not particularly pronounced. The variations shown in Fig. 8 are not understood.

The cascade intensity at a particular energy is dependent on the primary-beam energy for fixed primary beam current. The experimental evidence for this is shown in Fig. 9. The (negative) logarithm of $j(E)$ divided by the beam current i_B is plotted versus the logarithm of E_p for various values of E: 540 eV, 400 eV, 300 eV, and 200 eV. These values were selected so as to fall between energy values of potential Auger peaks (e.g., O, N, C, and S). As illustrated in the figure, the specimen normal was oriented at 45° with respect to the incident beam direction and 30° with respect to the analyzer axis. At all energies E a linear log-log relationship was found as E_p was varied between 2.2 and 3.0 keV. At lower energies nonlinear results occurred due to poor focusing behavior of the electron gun. The linear log-log result occurred with the same slope at all energies and can be expressed as

$$j(E) = bE_p^{-n}, \tag{20}$$

where $n = \tan 39° = 0.81$, for the data of Fig. 9. A power-law dependence on E_p is consistent with the Boltzmann equation, but a negative sign for the exponent is not.

We conclude from these results that a general expression for the cascade can be written as

$$j(E, E_p) = AE^{-m}E_p^{-n}, \tag{21}$$

where A is a constant. While n appears at this time to be independent of surface conditions it is

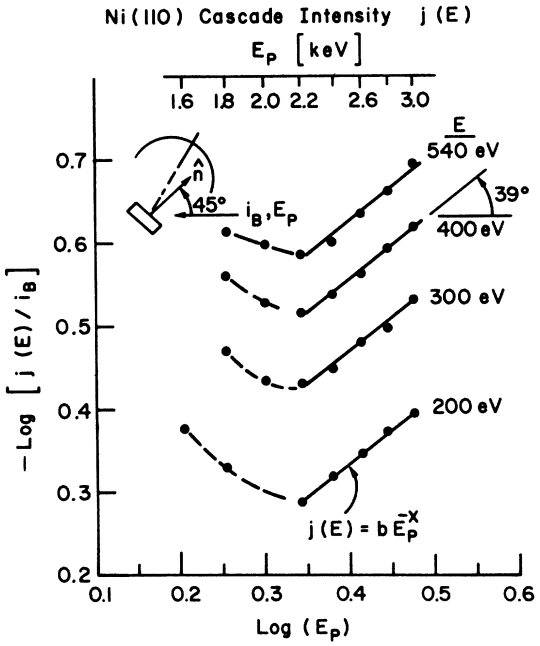

FIG. 9. (Negative) logarithm of the cascade intensities at fixed E plotted as a function of log E_p. The linear characteristic has the same slope (–tan 39°) in all four curves. The Auger spectrum showed a small carbon peak, a very faint sulfur peak, and no nitrogen or oxygen. The inset shows the orientation of the specimen relative to the primary beam and the analyzer.

found that m changes value between regions separated by Auger electron thresholds. In general, $|m|$ increases in regions of lower energy.

The observation that $d[\log j(E)]/d[\log E_p]$ is negative may be interpreted as a consequence of the energy dependence of the range of primary electrons. Range increases with energy while the rate of energy loss dE/dx at E_p decreases. With increasing E_p, passing primaries lose less energy in the surface region resulting in a diminished production of secondaries. Hence, in the surface region, $N(E)$ can be decreased with increasing E_p and so will $j(E)$. This implies that $N(E)$ is not homogeneous, but that a gradient exists in the surface region. In Wolff's analysis[14] the gradient of N is ignored in the Boltzmann equation. The gradient is sustained by the net loss of electrons at the surface in the form of the observed current $j(E)$ (see II).

V. DISCUSSION AND CONCLUSION

The linearity of the entire secondary-electron cascade associated with an external source of primary electrons, as hypothesized in Fig. 2, has not been tested directly. The reason is evident in all of the spectra shown, namely, that the primaries excite internal sources which also have associated cascades thus rendering the cascade (free of rediffused primaries) of an isolated external source a hypothetical concept. However, the segmented nature of the overall cascade, where segments are bounded by excitation thresholds for internal sources in consistent with expectations for multiple sources.

It is found that an effort to clean, *in situ*, the specimen surface is a prerequisite for observing a linear-cascade behavior. Without this effort the phenomenon may not be observed at all. In other words, the cleaner the specimen surface, the more linear will be the cascade. Segmenting, related to thresholds of bound electrons, identifies internal sources associated with the chemical composition of the surface region. Segmenting can be made to appear and disappear by adding or removing adsorbates. These effects are discussed in detail in II.

Linearization of the cascade in the energy range of shortest inelastic mean free paths has been demonstrated. To accomplish this it was necessary to investigate possible instrumental effects. Potential modulation of the retarding-grid analyzer is found to have proper modulation amplitude response. A possible source of inconsistency could occur when comparing cascade spectra having angular effects associated with the relative alignment of the electron beam, the specimen and the analyzer. This has been investigated and found to behave systematically in a reasonable fashion.

The sensitivity of the $\log j(E)/\log(E)$ mode of display to changes in surface composition is most pronounced. The quantification of this effect in terms of known surface coverages has not been accomplished as yet. However, comparisons of derivative displays, $dj(E)/dE$, with the $\log j(E)/\log(E)$ displays reveal interesting differences. The most obvious difference is that much smaller changes in slope between two linear segments are evident in the latter mode of display. It has been our experience, in general, that any Auger emission that can be detected in the derivative mode can be observed in the $\log j(E)/\log(E)$ mode, but the converse is not always true.

These observations constitute the basis for a new approach to surface studies in which emphasis is placed on observing segmenting of the linearized secondary-electron cascade. A number of interesting effects are presently under investigation by this method. In particular, it is now apparent that surface sources can be distinguished from subsurface sources. This is the subject of II.

Finally, it is noted that surface analyses based on the linearized cascade permit direct comparison of $j(E)$ intensity and line shape among several sources.

ACKNOWLEDGMENTS

It is a pleasure to recognize the able and extensive assistance from various associates that the author has enjoyed during this research. In particular, those who have assisted with the experimental details in the past several years are D. Ramano, S. Cunningham, and C. Kukla. The author is also grateful to W. Winterbottom, L. C. Davis, and C. Eagen for their continued interest and helpful discussions.

[1]C. N. Berglund and W. E. Spicer, Phys. Rev. 136, A1030 (1964); and 136, A1044 (1964).
[2]I. Lindau and W. E. Spicer, J . Electron Spec. Rel. Phen. 3, 409 (1974).
[3]C. J. Powell, Surface Sci. 44, 29 (1974).
[4]R. Kollath, Handb. Phys. 21, 232 (1956).
[5]R. D. Birkhoff, Handb. Phys. 34, 53 (1958).
[6]O. Hackenberg and W. Bauer, Adv. Electron. Electron Phys. 11, 413 (1959).
[7]L. C. Emerson, R. D. Birkhoff, V. E. Anderson, and

R. H. Ritchie, Phys. Rev. B 7, 1798 (1973).

[8]It is a popular practice in the current literature, especially among papers on Auger electron spectroscopy, to designate the observed emission current as $N(E)$; the number of electrons emitted at the surface with energy E. This can be a source of confusion when one wishes to distinguish an internal distribution $N(E')$ from an externally observable current $j(E)$. In general, these terms are related by the velocity as $j(E) = vN(E')$. This confusion will be avoided here by adopting the more conventional notation of $j(E)$ instead of $N(E)$ for the observed current and reserving the latter for the distribution function. Consequently, in comparing the experimental spectra shown herein with those reported elsewhere this distinction must be noted.

[9]E. N. Sickafus, Rev. Sci. Instrum. 42, 933 (1971).

[10]A. J. Dekker, *Solid State Physics* (Prentice-Hall, Englewood Cliffs, N. J., 1960), Chap. 17.

[11]A. J. Dekker, in *Solid State Physics Advances in Research and Applications*, edited by F. Seitz and D. Turnbull (Academic, New York, 1958), Vol. 6.

[12]M. P. Seah, Surf. Sci. 17, 132 (1969).

[13]E. N. Sickafus, Phys. Rev. B 7, 5100 (1973).

[14]P. A. Wolff, Phys. Rev. 95, 56 (1954).

[15]H. Stolz, Ann. Phys. (Leipz.) 3, 197 (1959).

[16]G. F. Amelio, J. Vac. Sci. Technol. 7, 593 (1970).

[17]A. J. Bennett and L. M. Roth, Phys. Rev. B 5, 4309 (1972).

[18]L. V. Spencer and V. Fano, Phys. Rev. 93, 1172 (1954).

[19]L. V. Spencer and F. H. Attix, Radiat. Res. 3, 239 (1955).

[20]R. H. Ritchie, J. Appl. Phys. 37, 2275 (1966).

[21]R. H. Ritchie, C. J. Tung, V. E. Anderson, and J. C. Ashley, Radiat. Res. 64, 181 (1975).

[22]Most of the data reported here were taken with a Varian Associates LEED system having a 96° aperture. Similar spectra have also been obtained with a Physical Electronics Industries LEED system having a 90° aperture.

[23]E. N. Sickafus and H. P. Bonzel, Prog. Surf. Membrane Sci. 4, 181 (1970).

[24]E. N. Sickafus, J. Vac. Sci. Technol. 11, 299 (1973).

[25]C. J. Powell, J. Vac. Sci. Technol. 13, 219 (1976).

[26]J. L. H. Jonker, Philips Res. Rep. 6, 327 (1951).

[27]J. R. Noonan, D. M. Zehner, and L. H. Jenkins, J. Vac. Sci. Technol. 13, 183 (1976).

[28]The graphs of Figs. 1, 5, 6, and 7 are photographic reproductions of the original 10-in by 15-in xy recorder traces.